PRODUCTION OF FLAT ELECTRON BEAMS AT THE FNPL

Tsatsu Nyamadi
Norfolk State University

Supervisor
Jamie Santucci
A0 Fermilab

May 19 - August 8, 2003

Abstract

Recently a new and less expensive technique for the production of an electron beam with a high transverse emittance ratio, "a flat beam," has generated substantial interest. This is because flat electron beams enable high luminosity with small space charge effects at the collision point. The technique is very pertinent due to the fact that it flattens an electron beam without large and expensive damping rings. A laser frees electrons from the cathode of an RF (radio frequency) gun, which is immersed in a solenoidal magnetic field. As a result, beams emitted from the round laser spot have a net angular momentum on exit from the solenoid. These beams are round at conception and are flattened by using a channel of quadrupole magnets. A comparison of experimental data with simulation was made. A transverse emittance ratio of 16.0 +/- 0.5 has been observed, and the result is in general agreement with simulations.

1   Introduction

Of late, there has been substantial interest in the use of flat beams for the next generation of linear colliders as well as for synchrotron light sources. Among the reasons cited for this are: firstly, flat electron beams allow for better center of mass energy distribution, and secondly, flat beams also enable high luminosity. Though there are other ways of producing flat beams, this particular method possesses numerous advantages due to the fact that it is less expensive and also less cumbersome. This technique, if developed, could result in the total elimination of the costly electron-damping rings currently used in linear collider design.

The purpose of this experiment is to demonstrate how to transform a round beam to a flat beam and compare the measured results with simulations. In the following sections, I

will present the principle of operation, a reduced version of the mathematical formalism, the Fermilab/NICADD[1] Photoinjector (shown in figure 1), and the quantity of emittance (used to measure the quality of a beam). An outline of the simulation method employed and a description of the experimental setup are provided. Finally, a discussion of the experiment and simulation results is presented and assessed.
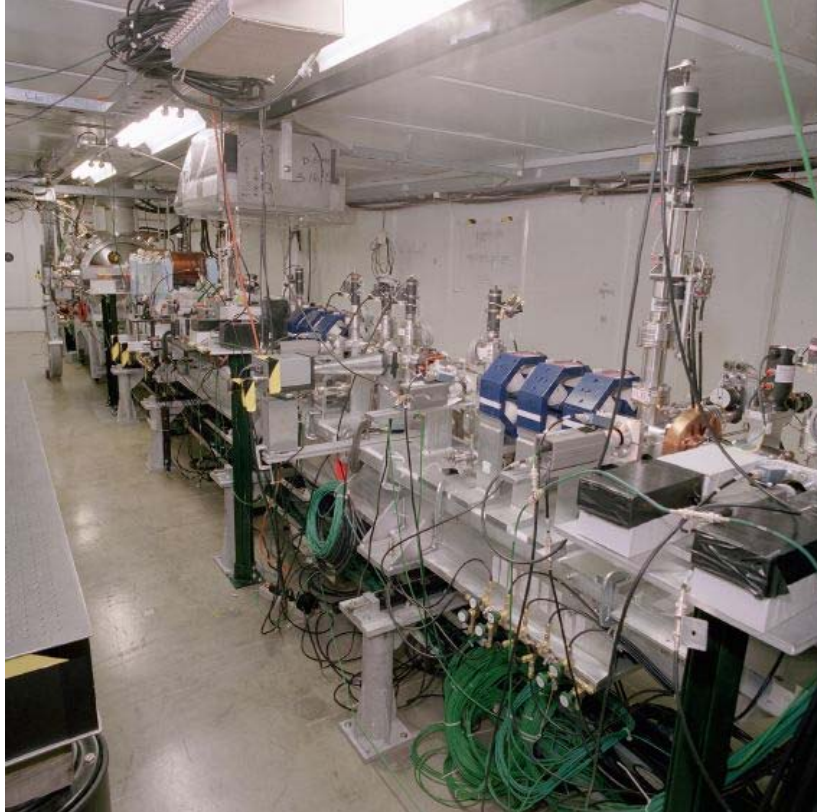
Figure 1: The Fermilab Photoinjector

2 Theory of Operation

The cathode of an electron gun is immersed in a solenoid that produces a magnetic field B_z, where z is the beam axis. A laser beam directed on the cathode frees a "bunch" of electrons. This bunch of electrons travels along the magnetic field lines of the solenoid as it undergoes acceleration within the gun, and nothing interesting happens

[1] Northen Illinois Center for Accelerator and Detector Development

until the end of the solenoid. Upon exit from this field, however, the beam acquires a kinetic angular momentum directed along the z-axis as shown in figure 2. A kinetic angular momentum is necessary to flatten the beam downstream.
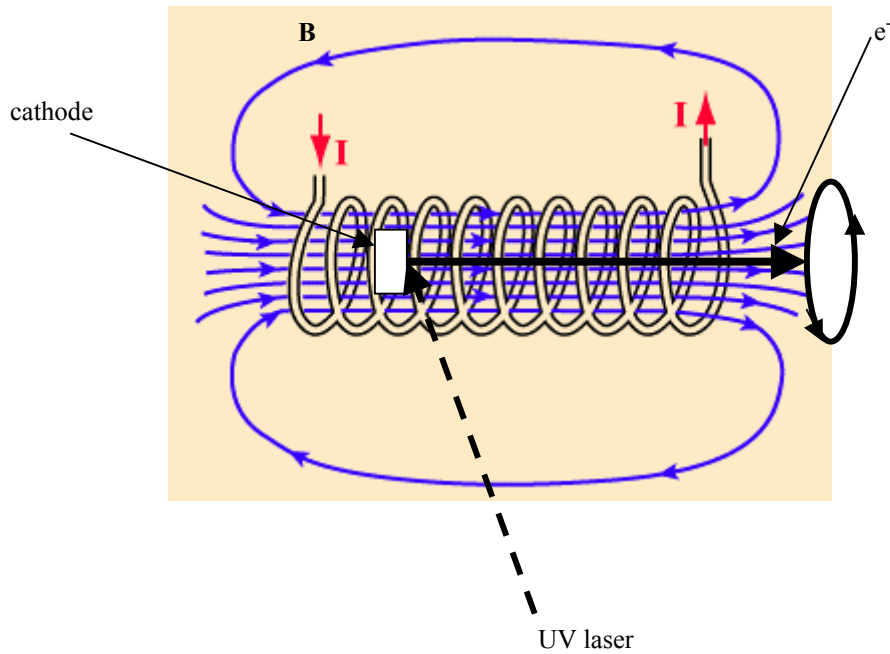
Figure 2: Solenoidal field with embedded cathode.

Consider a cylindrical coordinate system centered on the cathode. Assume the beam at the cathode has a zero transverse emittance i.e. the kinetic angular momentum is zero and the only momentum present is the canonical momentum. The canonical momentum P is given in equation (1).

$$\text{Canonical momentum } P = eA \qquad (1)$$

where A is the magnetic vector potential.
The magnetic vector potential A has an angular component obtained by Amperian loop as shown in figure 3.
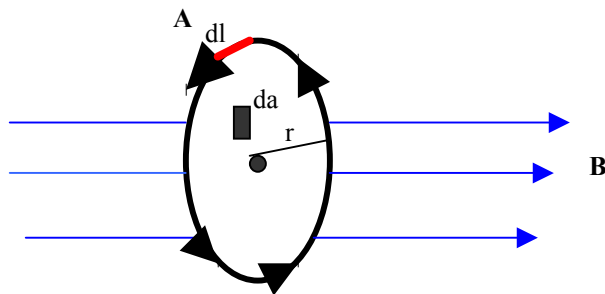
Figure 3: Amperian loop

This can be described mathematically by equation (2).

$$\oint A.dl = \int B.da \qquad (2)$$

where A = vector potential, B = magnetic field, l = circumference and a =area.

The interior magnetic field is uniform, so equation (2) reduces to equation (3).

$$A*2\pi r = B*\pi r^2 \qquad (3)$$

From equation (3), one finds

$$A = \frac{B}{2}r \qquad (4)$$

Using equation (3) and (4), the expression for the momentum P becomes,

$$P = e\frac{B}{2}r \qquad (5)$$

The transverse momentum is $P_t = e\frac{B}{2}r. \qquad (6)$

The spiral motion, (also known as vorticity), describes the deflection of the electron beam particles in the bunch. It follows that a particle having charge e and momentum Po exiting with transverse displacements $x = x_o$ and $y = y_0$ will be deflected through an angle in the y direction.

The deflections are defined as $x' = \dfrac{P_x}{P_z}$ and $y' = \dfrac{P_y}{P_z}$ \qquad (7).

Consider a vortex beam at the exit point shown in figure 4 below:
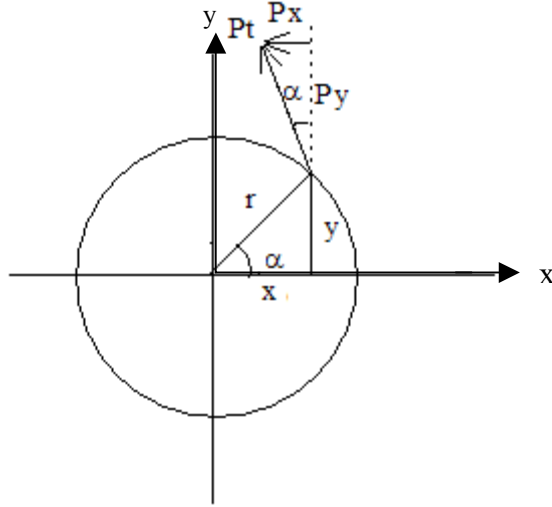
Figure 4: Vortex beam showing deflection

According to figure 4 we have,

$$Px = -P_t \sin\alpha$$
$$Py = P_t \cos\alpha$$

And also $\cos\alpha = \dfrac{x}{r}$ and $\sin\alpha = \dfrac{y}{r}$,

$$\Rightarrow \quad Px = -\frac{P_t}{r}y \quad \text{and} \quad Py = \frac{P_t}{r}x. \qquad (8)$$

Thus $Px \propto y$ and $Py \propto x$.

Upon combining (7) and (8), the expressions for the x' and y' become

$$\Rightarrow x' = -\frac{P_t}{P_z r}y = -ky \quad \text{and} \quad y' = \frac{P_t}{P_z r}x = kx \qquad (9)$$

From (6) and (9), $k = \dfrac{1}{2}\dfrac{eB_z}{pc}$.

Therefore a particle with initial transverse coordinates x_o and y_o acquires angular deflections. The initial state of the particle as it exits the solenoid becomes:

$$\begin{bmatrix} x \\ x' \\ y \\ y' \end{bmatrix} = \begin{bmatrix} x_o \\ -ky_o \\ y_o \\ kx_o \end{bmatrix}$$

To flatten the beam, the beam is passed through an alternating gradient quadrupole channel. The quadrupole channel can be represented by an identity matrix in the x-direction with an additional 90^0 phase advance in advance in y.

$$\begin{bmatrix} x \\ x' \\ y \\ y' \end{bmatrix} = \begin{bmatrix} 1 & 0 & 0 & 0 \\ 0 & 1 & 0 & 0 \\ 0 & 0 & 0 & \beta \\ 0 & 0 & \dfrac{-1}{\beta} & 0 \end{bmatrix} \begin{bmatrix} x_o \\ -ky_o \\ y_o \\ kx_o \end{bmatrix} = \begin{bmatrix} x_o \\ -ky_o \\ k\beta x_o \\ \dfrac{-y_o}{\beta} \end{bmatrix} \quad (10),$$

where β = constant associated with quadrupole channel. The choice of $\beta = \dfrac{1}{k}$ makes the particles end up with equal distances and angles in x and y. Assume four particles positions as shown in figure 5 below. The initial state of the particles is given by:

$$1: \begin{bmatrix} x \\ x' \\ y \\ y' \end{bmatrix} = \begin{bmatrix} 1 \\ 0 \\ 0 \\ 1 \end{bmatrix} \quad 2: \begin{bmatrix} x \\ x' \\ y \\ y' \end{bmatrix} = \begin{bmatrix} 0 \\ -1 \\ 1 \\ 0 \end{bmatrix} \quad 3: \begin{bmatrix} x \\ x' \\ y \\ y' \end{bmatrix} = \begin{bmatrix} -1 \\ 0 \\ 0 \\ -1 \end{bmatrix} \quad 4: \begin{bmatrix} x \\ x' \\ y \\ y' \end{bmatrix} = \begin{bmatrix} 0 \\ 1 \\ -1 \\ 0 \end{bmatrix}$$
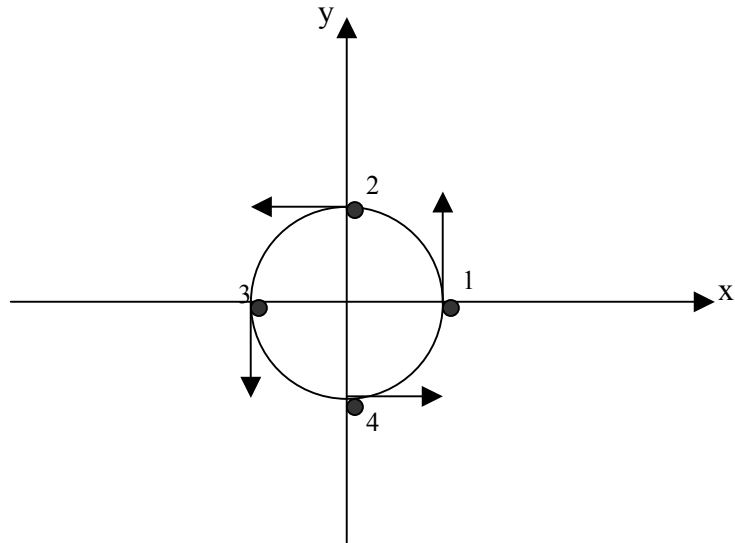
Figure 5: vortex beam

The flattening process can be illustrated by the application of quadrupole matrix to the four test particles at the end of the solenoid. Applying the matrix from equation (10) to all the positions of the vortex beam and plot the four test particles and after 45^0 ,the result is a flat beam shown in figure 6.
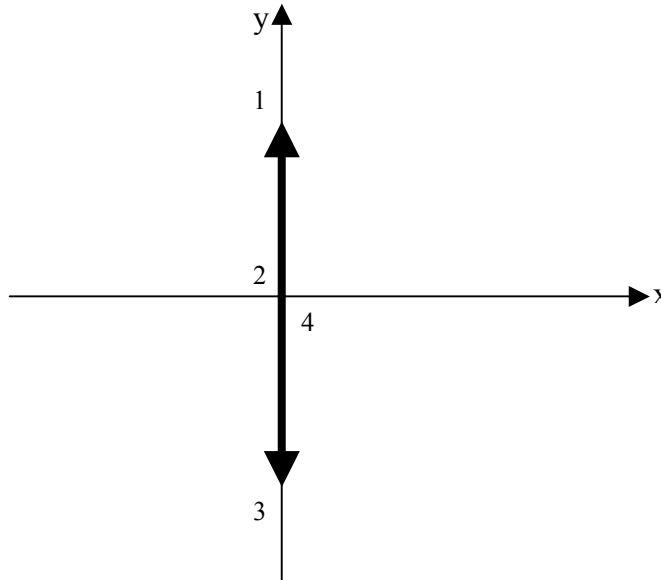
Figure 6: A flat beam

3 Procedure

The project was done experimentally and through simulation.

3.1 Experimental method: The Fermilab/NICADD Photoinjector is a linear accelerator that reaches a maximum energy of about 16 MeV. It is designed to produce high intensity low emittance electron beam. A pulsed 263nm UV laser is directed at a cesium telluride photo-cathode and electrons are ejected. A RF gun then accelerates the electrons to an energy of about 3.8 MeV. From there, a superconducting booster cavity raises the energy level to about 16 MeV. Attached to the superconducting cavity is an 8-meter beamline (as shown in figure 1) available for experiments. Guess and check methods were used to manipulate the quadrupole gradients to create a flat and stable beam.

  Having fixed the quadrupole gradients, and a flat beam is then produced.   As the beam travels down the beamline, flags utilizing optical transition radiations (OTR) are inserted at points XL6 and XL7 where beam images are obtained for emittance measurement. The

flag (made up of aluminum foil and glass) is inserted in the beamline at an angle of 45° to the beam axis (see figure 14). The aluminum foil emits light when struck by high-energy electrons.
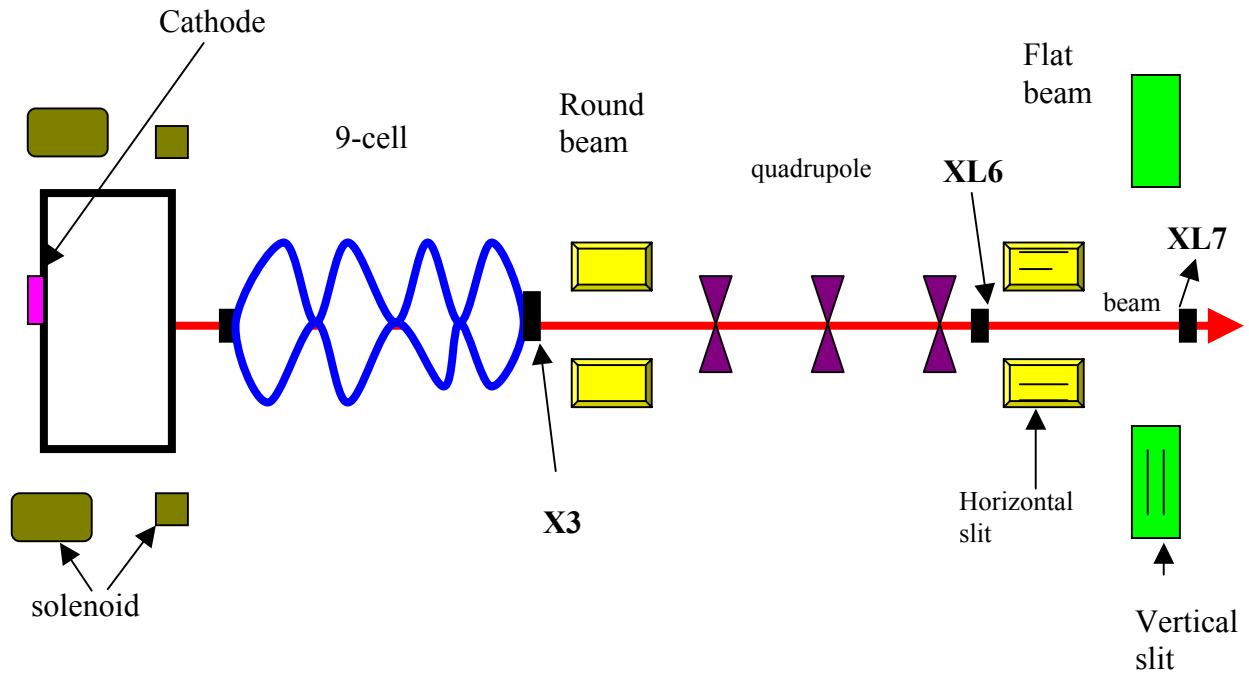
Figure 7: Schematic diagram of the Fermilab A0 layout

 A CCD camera (8-bit gray scale resolution) records the light emanating from the flag. Each image therefore is a snapshot of the transverse profile. The images are saved in tiff format for analysis. The aim here is to obtain the emittance (area of position and momentum space occupied by beam) ratio of the beam. The image of the beam taken at a position is referred to as position image and the image of the slit taken is referred to as momentum image. Position images are collected at a position called XL6 (end of third quadrupole) and horizontal and vertical slits are inserted at XL6 to obtain momentum images as per figure 10. Position images are obtained by using an OTR (Optical Transition Radiation) flag to measure beam image at XL7 and momentum images use OTR flag to measure slit image at XL7.The images obtained are analyzed using the Scion image analysis program.

σ_x measurement $\qquad\qquad\qquad\qquad$ $\sigma x'$ measurement

beam $\qquad\qquad\qquad\qquad$ flag $\qquad\qquad\qquad$ beam $\qquad\qquad\qquad\qquad\qquad\qquad$ flag

slit

camera

Beam imaging using OTR

Dispersion mersureement
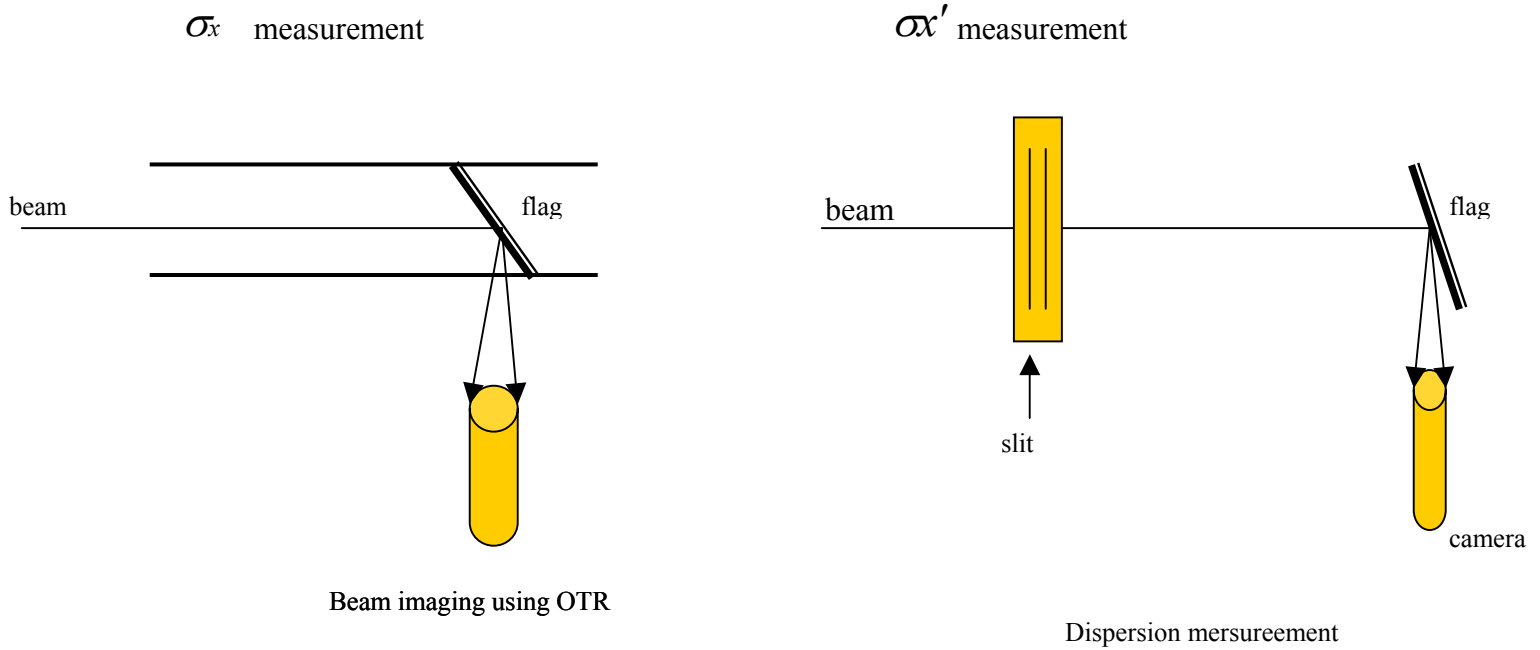
Figure 8: Beam imaging

The profiles of all the images were obtained and an rms (root mean square) value for the each image is computed. The rms value is then used to calculate the emittance ratio. This is because emittance is obtained from the product of the rms values of the two types of images.

3.2 Emittance $\mathcal{E}$: The quantity known as emittance is used to measure the quality of a beam. It refers to the area of position and momentum phase space occupied by a particle i.e. it simultaneously measures the beam's dispersion in position and momentum space as shown in figure 9. A beam with small emittance is desirable (as shown in figure 9), because it has a well-defined position and momentum and permits easy manipulation during collision.
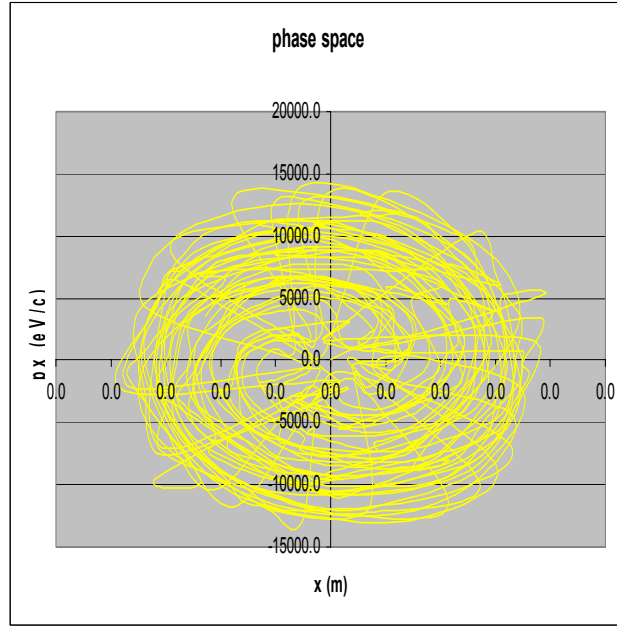
Figure 9: Emittance

The quantity emittance is defined longitudinally and transversely, but this paper deals exclusively with transverse emittance defined by equation   (9) as:

$$\mathcal{E}x \equiv \sqrt{\langle x^2 \rangle \langle x'^2 \rangle - \langle xx' \rangle^2} \qquad (9)$$

where x is the spatial coordinate and $x' = \dfrac{P_x}{P_z}$ is the transverse momentum dispersion.

Since there is no correlation between x and x' the correlation term is therefore neglected. Equation (9) then becomes equation (10).

$$\mathcal{E}x \equiv \sqrt{\langle x^2 \rangle \langle x'^2 \rangle} \qquad (10)$$

By symmetry: $\langle x \rangle = 0$ and $\langle x' \rangle = 0$.   (11)

So $\sigma_x{}^2 = \langle x^2 \rangle$ and $\sigma_{x'}{}^2 = \langle x'^2 \rangle$ (12)

where σ_x and $\sigma_{x'}$ refers to the root mean square (rms) values.

Simplifying further, equation (10) becomes

$$\mathcal{E}x = \sigma_x \sigma_{x'} \quad \text{measured in } mm\ mrad. \tag{13}$$

Emittance is generally recast as normalized emittance, in order to compensate for beam's energy (due to acceleration as it travels down the beam line). Normalized emittance is defined in equation (16) as:

$$\mathcal{E}_{normalized} = \beta\gamma\ \mathcal{E}, \tag{14}$$

where $\beta = \dfrac{v}{c} \cong 1$ and $\gamma \equiv 1 / \sqrt{1 - \dfrac{v^2}{c^2}} \cong 30$ shown in appendix 1.

The rms value (σ_x) is obtained from the image of the beam at position XL6 and $\sigma_{x'}$ is obtained from image of a slit at position XL6. The image of the beam obtained at positions XL6 and slit image obtained from the same position in this paper is referred to as position image and momentum images respectively.

3.3 Scion image program-Position Images: The first step is to average a couple of images to form a composite image of the beam spot. The images are considered as 2-dimensional arrays with a brightness-value assigned to each ordered pair of row and column. An individual image is denoted by i_{ij}, after averaging the composite image I becomes

$$I_{ij} = \frac{i_{ij} + ... + i_{nj}}{n} , \text{ where n = number of images.}$$

Additionally the average of a couple of background images were also obtained via the formula below:

$$B_{ij} = \frac{b_{ij} + ... + bm_j}{m}, \text{ where m = number of images.}$$

The background image is then subtracted from the final image of the beam spot. A corrected image obtained via:

$$J_{ij} = I_{ij} - B_{ij}.$$

The background correction removes hot spots, dark current, and other effects that can distort the beam profile. An example of a corrected background image as in figure 10 is then obtained.
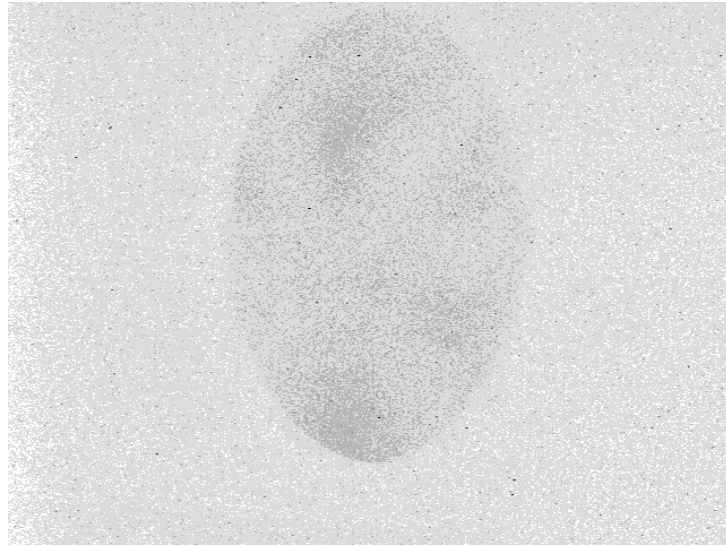
Figure 10: Background image **B**.

3.4 Scion image –Momentum image: The procedure is the same as that of position images with few additions. Here, a series of slits are inserted at the node after the quadrupole channel (also referred to as XL6), and a flag placed at XL7. The beamlets formed by the slit disperse at a rate proportional to their transverse momentum. The momentum spread is then extracted from the growth of beamlets width over the distance between the slits at XL6 and XL7. The slit images are averaged and corrected for background as shown in figure 10.
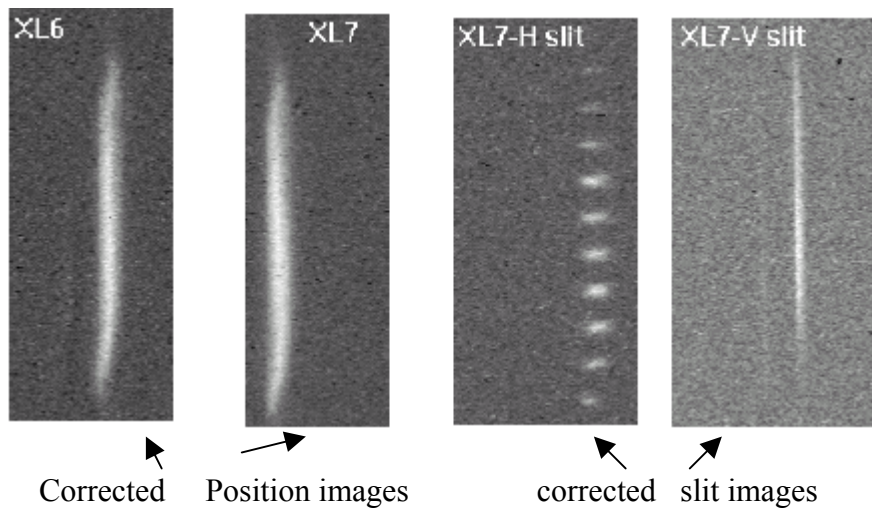
Figure 11: Selected images taken by camera

4   Simulation

4.1 A Space Charge Tracking Algorithm *Astra* is used to perform the simulation. Astra propagates a bunch of 500 charged particles through a three-dimensional space in discrete steps. At each step, it calculates the effects of user-defined external magnetic fields and also the internal space charge of the bunch itself. Astra then outputs a 500-row spreadsheet (for 500 particles) detailing the position and momentum of each particle at the end of a certain specified distance z as per table A.

Astra requires external magnetic field in order to simulate conditions in the beam line correctly. For flat beam experiments two different solenoids contribute to the B-field. The primary solenoid has a current I_p = 105A and secondary solenoid has amount I_s = 180A. Together they produce a magnetic field shown in figure 12 below:
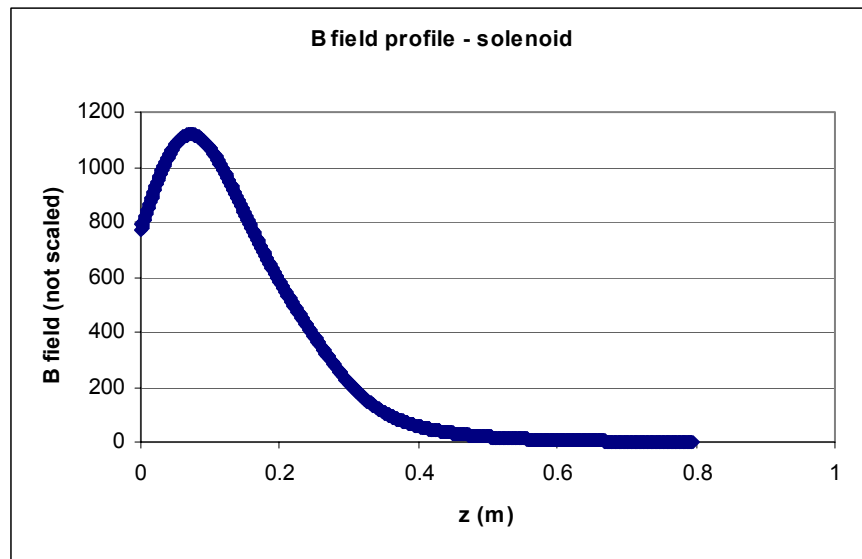
Figure 12: Solenoid profile

Particle	x(m)	y(m)	Z (m)	px(eV)	py(eV)
Reference	0.00E+00	0.00E+00	0.00E+00	0.00E+00	0.00E+00
2	1.46E-02	-2.803	-8.59^E-05	1.97E-05	-4.05^E+03
3	1.01^E-08	3.75^E-04	-3.50^E+00	1.45^E+00	-1.40^E+00
4	2.22^E-02	-1.01^E-02	2.81^E-03	2.9^E+04	-1.40^E+04

Table A: Sample Astra Output file

The simulation begins with the generation of the initial distributions of 500 particles as per table A. The particles are then propagated through the RF gun and the 9-cell cavity. Phase scans of the 9-cell cavity and RF gun cavities were performed to make sure they are tuned so as to produce bunches of the highest expected energy. The scans are then plotted as shown in figures 13 and 14.

phase scan - rfgun
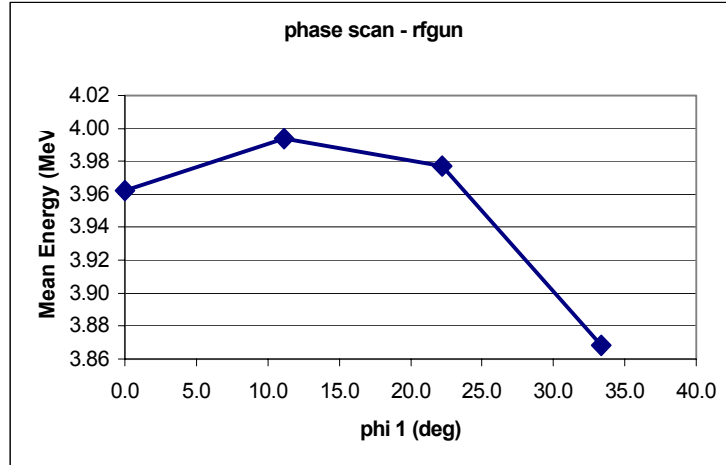
Figure 13: RF phasescan

Max energy occurs at about $\phi = 11^0$. This value is set in the Astra file to ensure the generation of max energy.

Mean energy vs. phi 2 ----9-cell phasescan
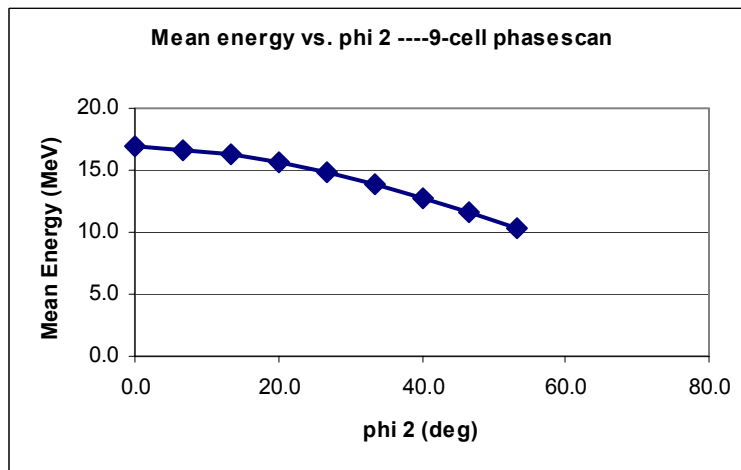
Figure 14: 9-cell phasescan shows max energy of 16 MeV at $\phi = 0^0$.

Solenoid focusing must take place before the particles can be propagated up to the quadrupole channel. This is because a well-focused beam has a better-defined correlation matrix from which the quadrupole gradients are extracted. The beam is therefore focused, by varying the solenoidal fields at the cathode until a spot size at X3 = 3.95m is minimized. A plot of the well-focused beam is shown in figure 15.
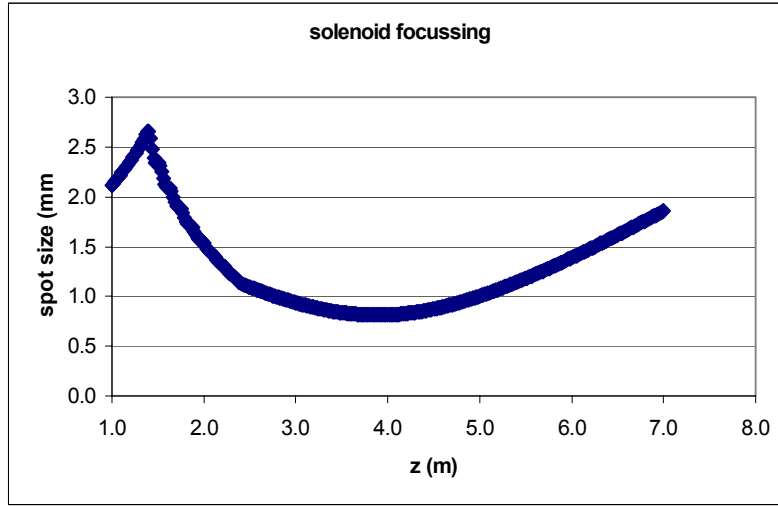
Figure 15: Properly focused solenoid min at X3.

4.2 Correlation Matrix C. The vorticity of the beam ensures correlation of the canonical coordinates x = (x, x') and y = (y, y'). This is used to develop a model for the flattening process. The correlation matrix C relates a particle's position and momentum in the x-direction to its position and momentum in the y-direction as it travels down the beam line. C is defined as:

$$\begin{pmatrix} y \\ y' \end{pmatrix} = \begin{pmatrix} c_{11} & c_{12} \\ c_{21} & c_{22} \end{pmatrix} \begin{pmatrix} x \\ x' \end{pmatrix} \tag{15}.$$

where $x' \equiv \dfrac{P_x}{P_z}$ and $y' \equiv \dfrac{P_y}{P_z}$.

Under general conditions, C is of the form $C = \begin{pmatrix} a & b \\ \dfrac{-1+a^2}{b} & -a \end{pmatrix}$.

Once the beam is properly focused, the simulation process is continued with quadrupole tuning. The correlation matrix is extracted from post-acceleration output file as per equation (11). In the simulation C was determined to be:

$$C = \begin{pmatrix} 0.055 & 1.618 \\ -0.585 & -0.038 \end{pmatrix}$$

4.3 Quadrupole channel. The transformation is formed by three skew quadrupoles. A single quadrupole magnet can be modeled as four bar magnets. The arrangement of the poles "squeezes" the beam in one direction and "stretches" it in another direction as shown in figure 16.
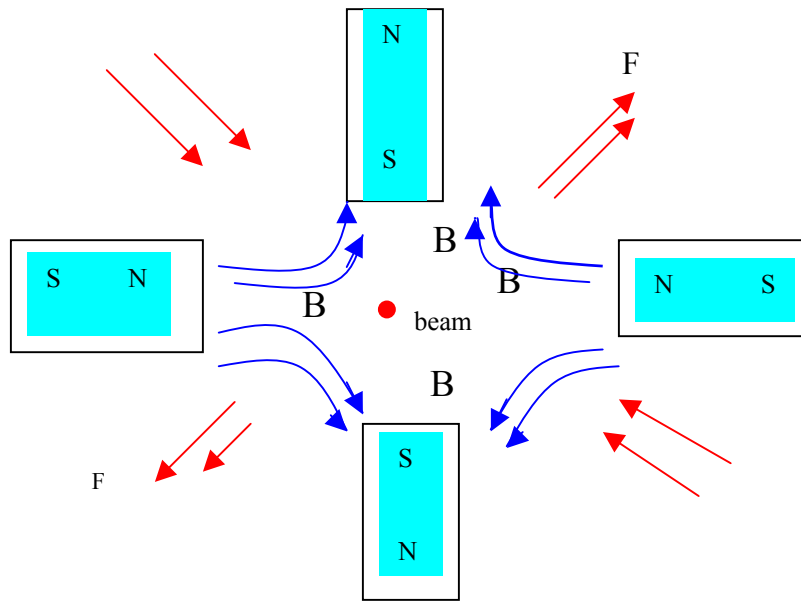
Figure 16: Quadrupole flattening

The quadrupole flattens the beam, but the newly flattened beam is radially unstable. A second quadrupole magnet is required to prevent the beam from flying apart. The second magnet therefore removes the destabilizing radial momentum from the beam. A third quadrupole rotates the angle of the stabilized flat beam.

Two types of matrices are used to characterize the effect of quadrupole channel on an electron bunch. A drift matrix transforms the particle's position and momentum coordinate to reflect its field-free drift of a distance *d* as shown in figure 16 below:
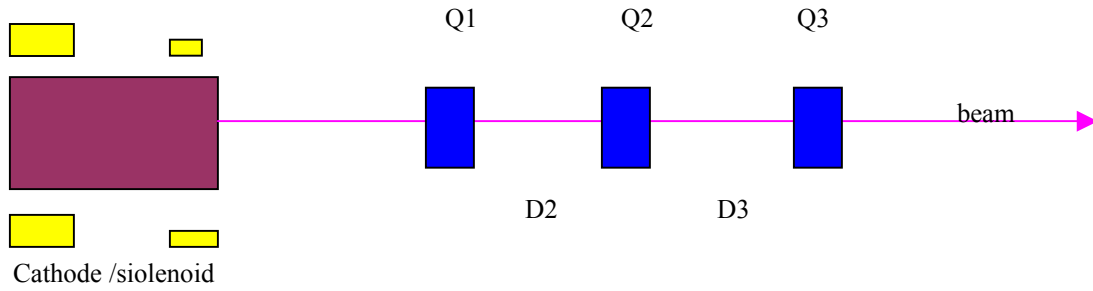
Figure 17: The Quadrupole channel

$$Dx = \begin{pmatrix} 1 & d \\ 0 & 1 \end{pmatrix} \begin{pmatrix} x \\ x' \end{pmatrix}_i = \begin{pmatrix} x \\ x' \end{pmatrix}_f \qquad (16)$$

Using the thin lens approximation, the effect of quadrupole magnet with gradient q is given by

$$Qx = \begin{pmatrix} 1 & 0 \\ q & 1 \end{pmatrix} \begin{pmatrix} x \\ x' \end{pmatrix}_i = \begin{pmatrix} x \\ x' \end{pmatrix}_f \qquad (17)$$

The entire quadrupole channel is modeled as a product of all the quadrupole and drift matrices:

$$x_f = Q_3 D_3 Q_2 D_2 Q_1 x_i \equiv A x_i \qquad (18).$$

The final matrix **A** defines the transport matrix for the canonical x-coordinate. Notice that the drift distance d_2 and d_3 are constants, which can be measured directly from the beamline. In this experiment $d_3 = 2.05\text{m}$ and $d_2 = 0.507\text{m}$

Similarly, a transport matrix similar to **A** called **B** describes the influence of the quadrupole channel on the y- coordinate.

$$B \equiv P_3 D_3 P_2 D_2 P_1$$

P is the same form as Q but with a negative gradient:

$$P = \begin{pmatrix} 1 & 0 \\ -q & 1 \end{pmatrix} \tag{19}$$

The requirement that the beam quadrupole is flat and devoid of angular momentum means:

$$y_f = x_f \tag{20}$$

But this condition has two components. First,

$$y = x \tag{21},$$

ensures that the particle lies on a line $45°$ up from the x-axis and, second

$$y' = x' \tag{22},$$

ensures no angular momentum remains.

From the definition of the correlation matrix as expressed in equation (15), we then obtain

$$\mathbf{A} = \mathbf{B}C \tag{23},$$

where C is the familiar correlation matrix.

This equation yields four equations with three unknowns (q1, q2, q3) each per quadrupole gradient. The solution to this equation, derived by Don Edwards at AO Fermilab, is:

$$q_1 = \sqrt{\frac{-D_2 c_{11} + D_2(D_2 + D_3)c_{21} + (D_2 + D_3)c_{22}}{D_2(D_2 + D_3)c_{12}}}$$

$$q_2 = \frac{c_{12} + (D_2 + d_3)C_{22}}{D_2 D_3(1 + q_1 c_{12})}$$

$$q_3 = \frac{-q_1 - q_2 - D_2 q_1 q_2 c_{11} - c_{21}}{1 + [(D_2 + D_3)q_1 + D_3 q_2]c_{11} + D_2 D_3 q_2 (q_1 + c_{21})}$$

During the experiment, C is not known; hence quadrupole settings are not known either. To find the quadrupole gradients, the quadrupole magnets are tuned by guess-and check until a flat beam is obtained. From equation 11, we then determine the average value of C for all the particles in the beam. In the simulation however, we can directly obtain C and use it to get the quadrupole settings. The quadrupole settings are then used to obtain a predicted emittance for the simulation. This value will then be conveniently compared with the experimental value.

A different program is then used to calculate the quadrupole predictions via equation (11). The quadrupole magnets are then programmed according to these predictions and the bunch is propagated through the quadrupole channel. Astra computes a final output file containing emittance. The measured quadrupole gradients are shown in table **B** below. The graph of *x* and *y* emittance is plotted against *z* (beam distance) in figure 18:
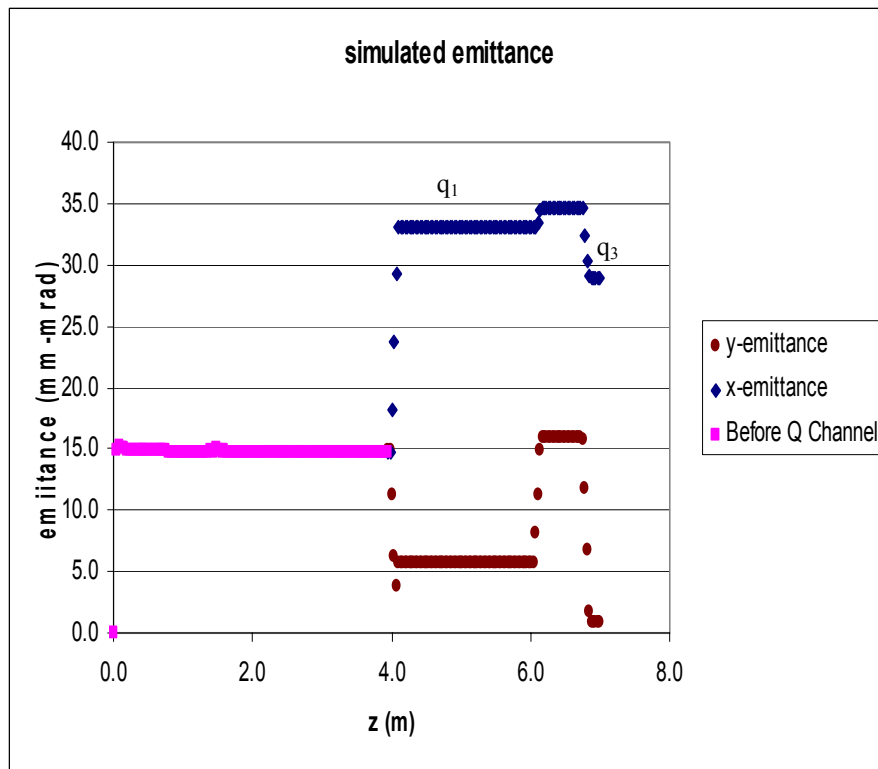
Figure 18: Emittance ratio

5   Results and Analysis

The vertical and horizontal profiles of the position image and the slit images were obtained, (see figures 20 and 21).
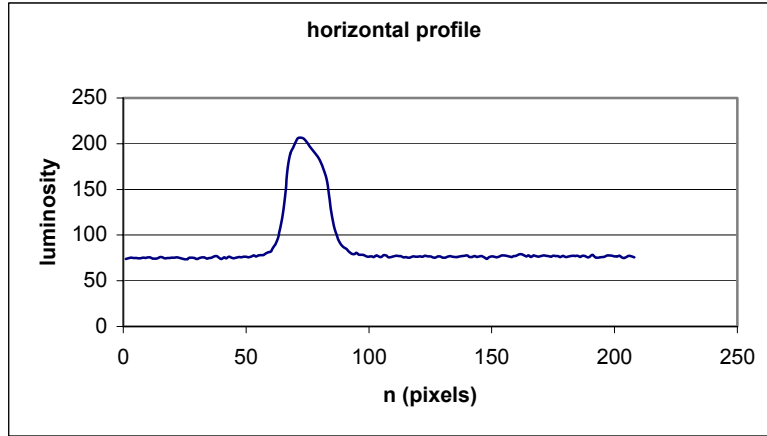
Figure 19: Flat beam
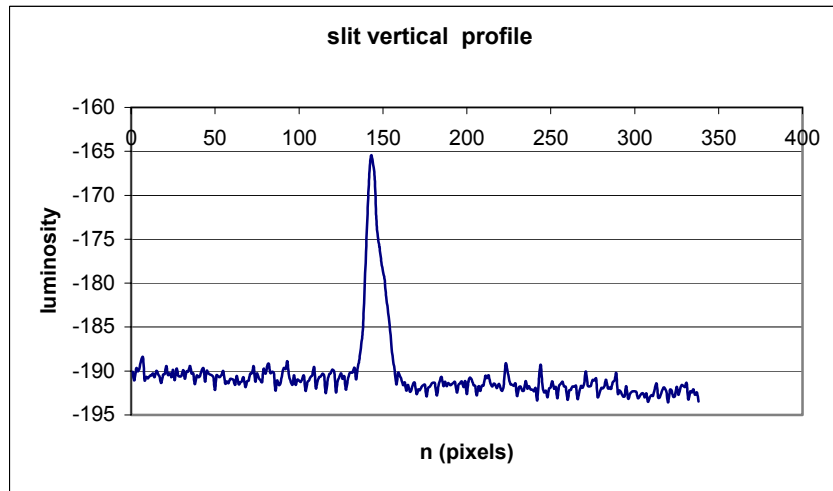
Figure 20: Slit profile

Recall the definition of emittance,

$$\mathcal{E}_{normalized} = \beta\gamma\, \mathcal{E}x \text{ , where } \mathcal{E}x = \sigma_x\sigma_{x'}$$

σ_x is obtained from the profile of the position image pixels taking into account the ratio of pixel to microns (µm) at XL6.

Also $\sigma_{x'}$ = arctan $\dfrac{\sigma_w}{d}$ assuming the slit size is very small and d = distance between slit and camera and σ_w.

The same procedure is repeated slit image each profile.

=> $\mathcal{E}x$ = $\sigma_x\sigma_{x'}$ which is the emittance in the x-direction and also

$\mathcal{E}y$ = $\sigma_y\sigma_{y'}$ which is emittance in the y-direction. The results of the simulation and experiment are displayed in table C.

	σ X3 (mm)	Ip (A)	Is (A)	i_1 (A)	i_2 (A)	i_3 (A)	$\mathcal{E}x$ (mm-mrad)	$\mathcal{E}y$ (mm-mrad)	$\dfrac{\mathcal{E}x}{\mathcal{E}y}$
Experiment.	0.95	105	180	0.60	0.31	0.22	1.68	27.26	16
Simulation	0.814	117	180	0.82	0.56	0.47	0.86	28.8	33.4

Table C: Final emittance

6 Conclusion

The measurements indicated an emittance ratio of 16.0 for the experiment; the Astra simulation was 33.4. Looking at the two results, the agreement between experiment and simulation is less than perfect but the principle of round-to-flat beam transformation has been verified. The reason for the disparity is attributable to the fact that there are

variations in the bunch and space charges. In addition, there are hot spots in the beam spot and experimental errors were not accounted for.

7 Acknowledgements

I want to thank my supervisor, Jamie Santucci, for his insights, assistance, and his patience in guiding me though this project. I also want to thank Helen Edward and Don Edwards for their support and the confidence they had in me that I could do this experiment. My thanks also goes Kai Desler, Daniel Mihalcea, Phillipe Piot and Yin-e Sun for the help and knowledge that I have acquired from them. Finally my thanks goes to the Fermilab A0 group for their support and encouragement especially Eric Thrane (my mentor) and Jason Wennerberg. Last but not the least, I want to thank Dianne Ingram, Elliot McCrory, James Davenport, and the rest of SIST committee for giving me another opportunity to be here and their help during my period here.

8 References

[1] D. Edwards et al, "The Flat beam experiment at FNAL Photoinjector", Proceedings LINAC2000.

[2] D. Edwards et al, "The Flat beam experiment at FNAL Photoinjector", Proceedings LINAC2001.

[3] E. Thrane "Flat Electron Beam Dynamics: A comparison of Data with Simulation", Thesis W.L Prize Competition 2003.

9 Appendix

<u>Appendix I</u>. Proof of $\gamma = 30$.

Define the rest energy $E_0 = mc^2$,

The total energy (rest energy + kinetic energy) $E = \gamma mc^2$.

Thus the Lorentz factor γ is the ratio of the particle's total energy to its rest energy

$$\gamma = \frac{E}{E_0}$$

$E_0 = 0.5$ MeV and $E = 15$ MeV so,

$$\gamma = \frac{15}{0.5} \cong 30.$$